Conductivity Imaging of Human Lower Extremity using MREIT with Multi-echo Pulse Sequence and 3 mA Imaging Current

Young Tae Kim, Atul S. Minhas, Zijun Meng, Hyung Joong Kim, and Eung Je Woo
Impedance Imaging Research Center and Department of Biomedical Engineering
Kyung Hee University
Gyeonggi-do, Korea

***Abstract*—We present our recent developments in tissue conductivity imaging of the human lower extremity using MREIT. In performing *in vivo* human knee and calf imaging experiments, we addressed two technical issues of the chemical shift artifact and measurement noise. Adopting a recently developed chemical shift artifact correction method for MREIT, we could improve the quality of conductivity images of the knee and calf. We found that the correction method is advantageous in terms of the signal-to-noise ratio (SNR) compared with a fat suppression method. Since the knee is more sensitive to injection currents, we limited the current amplitude in knee experiments to 3 mA to avoid painful sensation. Reduction of the current amplitude requests a similar reduction of the noise level in measured magnetic flux density signals since the signal is proportional to the current amplitude. We incorporated a lately developed multi-echo based MREIT pulse sequence to enhance MR signals and prolong the total current injection time, thereby reducing the noise level in measured magnetic flux density signals.**

Keywords-MREIT, conductivity image, magnetic flux density, chemical shift artifact correction

I. INTRODUCTION

Though the recent progress in MREIT has been reducing the injection current amplitude, it is still in the range of a few milliamperes. At this level, it is more sensible to initiate *in vivo* human MREIT imaging by choosing the extremity as an imaging region. The human lower extremity includes muscles, membranes, synovial fluids, bones, bone marrow, and fatty tissues. The first *in vivo* human MREIT experiment of the calf has revealed two technical issues of the chemical shift artifact and noise in B_z images [1].

The chemical shift occurs in fat regions and results in misalignments of pixels along the frequency encoding direction. Reconstructed conductivity images using such data suffer from artifacts originated from signal void at one side and overlap at the other. Fat suppression methods should be avoided in MREIT since they weaken MR signals which carry information on the induced magnetic flux B_z. Acquiring k-space data at a wider bandwidth is also undesirable due to an increased noise level in MR signals. In MREIT, we should use a chemical shift artifact correction method which can remove the artifact in both MR magnitude and phase images.

Given an MRI scanner and RF coils, data averaging is generally tried to reduce random noise at the cost of a prolonged scan time. The noise level in a B_z image is inversely proportional to the product of the MR magnitude image SNR and the total current injection time [2,3]. Lately, multi-echo based MREIT pulse sequences were suggested to utilize a remaining time after the first echo within one TR to obtain more echo signals and also to prolong the total current injection time [4,5]. This method is advantageous for an imaging region with large T2 values since a slow T2 decay results in useful secondary and other echo signals. Compared with the calf, we found that the knee is more sensitive to injection current with a pain threshold of about 3.5 mA. Fortunately, we found that T2 values of the knee region are long enough for a multi-echo pulse sequence. Following the first human trial by Kim *et al.* [1], in this paper, we present further developments in *in vivo* human imaging experiments including the chemical shift artifact correction and multi-echo methods.

II. METHODS

A. Subjects and Current Source Setting

Six healthy volunteers (three for calf and three for knee imaging) participated in the imaging experiments. Three male and three female subjects (subject A to F) were 25 to 30 years old. The experimental protocol was the same as the one described by Kim *et al.* [1] and approved by the institutional review board (IRB). We attached four carbon-hydrogel electrodes around the calf or knee as shown in Fig. 1 (a) and (b). We chose one pair of opposite electrodes to inject current. We gradually increased the current amplitude from zero mA to a pain threshold. We recorded current amplitudes at thresholds of sensation and pain. After repeating the same procedure for the other electrode pair, we determined the imaging current amplitude as 95% of the smaller pain threshold. Table 1 summarizes the current source setup for the six subjects. After this setup, we placed the subject inside the bore of our 3T MRI scanner (Magnum 3, Medinus Co. Ltd., Korea) with the four electrodes connected to a custom designed MREIT current source [6].

978-1-4244-8281-8/11/$26.00 ©2011 IEEE

TABLE I. CURRENT SOURCE SETUP FOR SIX HUMAN SUBJECTS. HORIZONTAL AND VERTICAL CURRENT INJECTION DIRECTIONS ARE DENOTED AS H AND V, RESPECTIVELY.

Normal volunteer	Knee						Calf					
	Subject A		Subject B		Subject C		Subject D		Subject E		Subject F	
Injection direction	H	V	H	V	H	V	H	V	H	V	H	V
Sensation threshold [mA]	1.0	1.0	1.0	1.5	1.5	1.0	1.5	1.0	1.5	1.5	2.0	1.5
Pain threshold [mA]	4.0	3.5	3.5	3.5	3.5	4.0	10.5	10.0	10.0	9.5	10.0	10.0
Imaging current amplitude [mA]	3.0	3.0	2.5	2.5	3.0	3.0	9.0	9.0	8.0	8.0	9.0	9.0

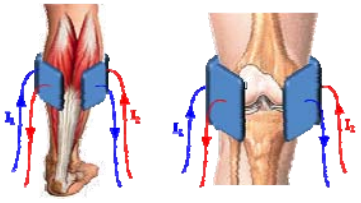

Figure 1. Attachment of carbon-hydrogel electrodes on the calf and knee.

B. *Chemical Shift Artifact Correction*

In calf experiments, we used the injection current nonlinear encoding (ICNE) pulse sequence with a single echo [7]. As shown in Table 1, the injection current amplitude was 8 or 9 mA which was below the pain thresholds. Short T2 values of the calf region prevented us from using a multi-echo pulse sequence which could have reduced the current amplitude.

We had to limit the current to 3 mA for the knee since it is more sensitive to electrical current. If we had used the single-echo ICNE for the knee, we should have significantly increased the total scan time to reduce the noise level in B_z images. Fortunately, T2 values of the knee region were long enough and we could adopt a multi-echo pulse sequence incorporating three echoes [4,5]. Table 2 summarizes imaging parameters for both calf and knee experiments. For knee experiments, we listed injection current pulse widths of three echoes individually.

In order to collect three Dixon data sets for the chemical shift artifact correction [8], we modified both single-echo and multi-echo pulse sequences. For each echo signal, we collected three Dixon data sets with three read gradient shifts of (- π, 0, +π) and performed the chemical shift artifact correction. In the multi-echo pulse sequence, we therefore performed the chemical shift artifact correction three times separately for three echo signals. In order to enhance the SNR in B_z images of the knee, we added phase changes accumulated throughout the entire current injection time by multiplying the corrected three echo data together. Using two pairs of opposite electrodes, we obtained artifact-free multi-slice B_z images subject to two injection currents at different directions.

C. *Conductivity image reconstruction*

From two sets of multi-slice B_z images subject to two injection currents, we reconstructed cross-sectional conductivity images using the MREIT software package called CoReHA [9]. Since the harmonic B_z algorithm [10] implemented in CoReHA assumes an isotropic conductivity distribution, we should interpret a conductivity image in this paper as an equivalent isotropic conductivity image.

TABLE II. IMAGING PARAMETERS FOR KNEE AND CALF EXPERIMENTS.

Imaging parameter	Knee			Calf
	Echo 1	Echo2	Echo 3	Single echo
TR (Repetition time, ms)	900	900	900	1000
TE (Echo time, ms)	30	60	90	30
Sampling time (μs)	24	24	24	24
FOV (mm^2)	200	200	200	180
Pixel size (mm)	1.56	1.56	1.56	1.41
Current injection duration (ms)	28	56	84	29

III. RESULTS

Fig. 2 illustrates a result of water-fat separation in the human knee experiment. The uncorrected MR magnitude image of the knee in (a) shows signal void and signal overlap due to the chemical shift. The separated water and fat images are shown in (b) and (c), respectively. Four hydrogel electrodes, muscles and synovial fluid around bones appeared in the water image. The subcutaneous adipose tissues and red bone marrow appeared in the fat image. The corrected artifact-free image is shown in (d).

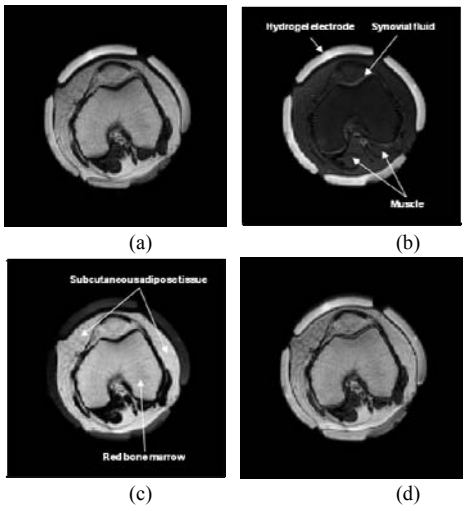

Figure 2. Water-fat separation of MR magnitude images of the knee with four carbon-hydrogel electrodes attached around it. (a) is the uncorrected image with chemical shift artifacts, (b) is a water image, (c) is a fat image, and (d) is a corrected image including both water and fat signals.

Fig. 3 shows MR magnitude, magnetic flux density (B_z), and reconstructed conductivity images of the knee. Images in (a-c) and (d-f) were obtained without and with the chemical shift artifact correction, respectively. Fig. 3(b) and (c) show spurious noise spikes which are significantly reduced in (e) and (f) after applying the chemical shift artifact correction. We marked in (f) by arrows locations of significant noise reduction. Fig. 4(a) shows multi-slice MR magnitude images of the knee after the correction. Reconstructed conductivity images without and with the correction are shown in (b) and (c), respectively.

Identify applicable sponsor/s here. *(sponsors)*

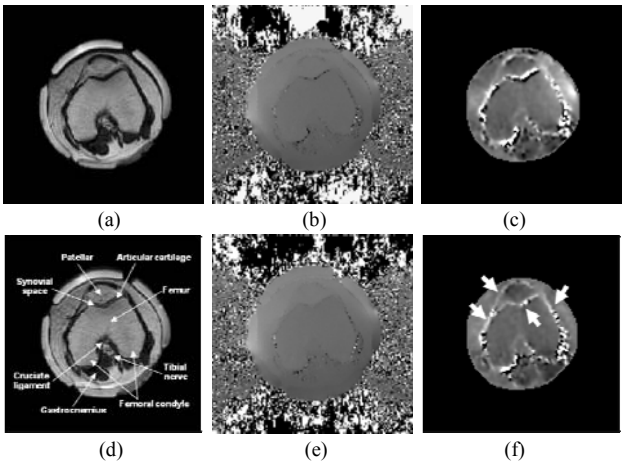

Figure 3. Typical MREIT images of the knee without and with the chemical shift artifact corrections. (a)-(c) are MR magnitude, B_z, and reconstructed conductivity images, respectively, without the chemical shift artifact correction. (d)-(f) are the corresponding images after the correction. The typical anatomical structure of the knee is labeled in (d). Arrows in (f) indicate regions of a significant conductivity contrast improvement and noise removal by using the chemical shift artifact correction.

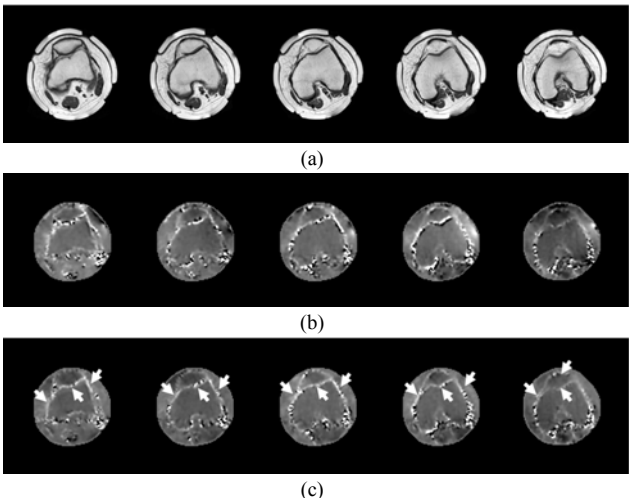

Figure 4. (a) Multi-slice MR magnitude images of the knee. (b) and (c) are reconstructed conductivity images without and with the chemical shift artifact correction, respectively. Arrows in (c) indicate regions of a significant conductivity contrast improvement and noise removal by using the chemical shift artifact correction

Fig. 5 shows MR magnitude, B_z, and conductivity images of the calf. MR signal void has occurred in the ring-shaped cortical bone of the tibia primarily due to the lack of protons and we should expect noisy pixels within such a ring-shaped region in both B_z and conductivity images. In the uncorrected images in (a-c), the shifting of adipose fatty tissues into the cortical bone region resulted in artifacts in B_z and conductivity images. After the correction in (d-f), the noise pattern matches well with the ring-shaped cortical bone. We can also see enhanced conductivity contrast around the crural fascia and intermuscular septum which is not clearly observed in the uncorrected images. Fig. 6(a) shows multi-slice MR magnitude images of the calf after the correction. Reconstructed conductivity images without and with the correction are shown in (b) and (c), respectively.

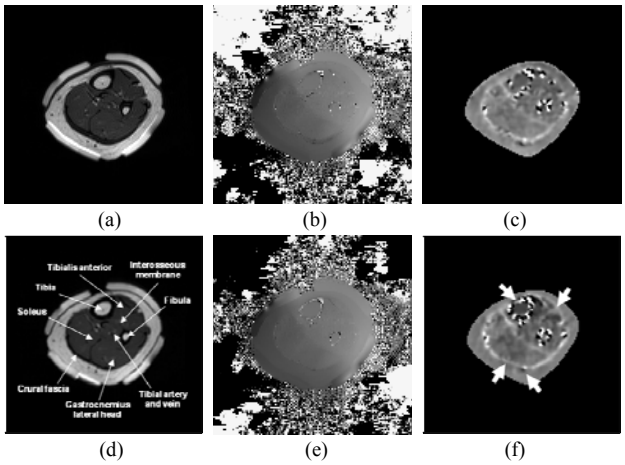

Figure 5. Typical MREIT images of the calf without and with the chemical shift artifact corrections. (a)-(c) are MR magnitude, B_z, and reconstructed conductivity images, respectively, without the chemical shift artifact correction. (d)-(f) are the corresponding images after the correction. The typical anatomical structure of the calf is labeled in (d). Arrows in (f) indicate regions of a significant conductivity contrast improvement and noise removal by using the chemical shift artifact correction.

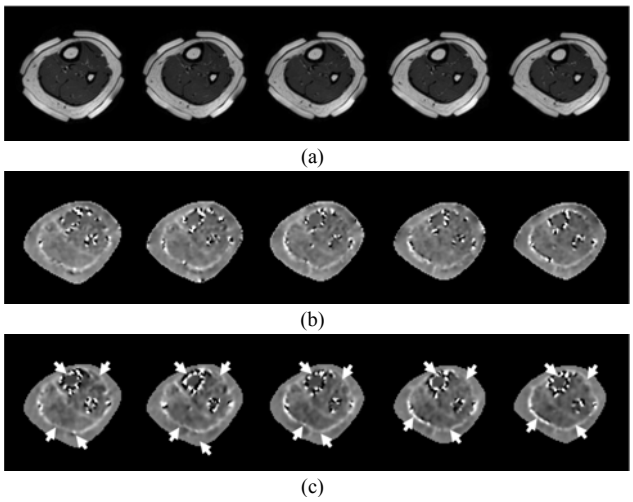

Figure 6. (a) Multi-slice MR magnitude images of the calf. (b) and (c) are reconstructed conductivity images without and with the chemical shift artifact correction, respectively. Arrows in (c) indicate regions of a significant conductivity contrast improvement and noise removal by using the chemical shift artifact correction

IV. Discussion and Conclusion

The issue of the chemical shift artifact reported in a previous human MREIT imaging experiment has been resolved in this study by adopting a customized correction scheme [8], which is based on the three-point Dixon's water-fat separation method [11,12]. Using the scheme proposed by Minhas *et al.* [8], we could successfully separate water and fat signals in both MR magnitude and phase images.

In the uncorrected MR magnitude image of the knee, the high MR signal of the synovial fluid was mixed with the fat signal. Moreover, signal void and overlap due to the chemical shift appeared in the regions between subcutaneous adipose tissues and hydrogel electrodes. Separated water images correctly showed MR signals of the muscle, synovial fluid, and four hydrogel electrodes whereas subcutaneous adipose tissues and red bone marrow appeared in fat images. After combining the water image with the corrected fat image, the synovial fluid and subcutaneous adipose tissues underneath hydrogel electrodes were relocated at their original positions (Fig. 2).

Without using the correction method, the conductivity image around the femur showed a spurious noise pattern due to MR signal overlap and void caused by the chemical shift. The exact localization of fat signals using the correction method recovered a conductivity contrast among the adipose tissues, femur, and synovial fluid. Since the adipose tissues around the knee were a mixture of fat, body fluids, and blood [13], their conductivity values appeared to be higher than that of the femur. The epiphysis of the femur was a cancellous bone. Since cancellous bones are highly vascular and contain red bone marrow [13], the epiphysis appeared to be more conductive than the muscle.

The calf consists of muscles, bones, and subcutaneous adipose tissues. The main differences between the calf and knee are the amount of muscles and the type of bones [13]. The diaphysis of the tibia and fibula in the calf is made up of a ring-shaped cortical bone and usually contains bone marrow and adipose tissue [13]. Before the chemical shift artifact correction, we could not see the ring-shaped noise pattern in the cortical bone of the tibia since the noise was reduced by the shifting of adipose fatty tissues into the cortical bone region. After the correction, the noise pattern matched well with the shape of the cortical bone, where MR signal void occurred due to the lack of protons. The adipose tissues around the calf showed slightly higher conductivity values than the transversal conductivity of the muscle and we speculate that this stems from body fluids and blood inside the adipose tissues in their *in vivo* wet state. The bone marrow had conductivity values smaller than that of the muscle in the calf and we speculate this is due to the presence of fat in the bone marrow. The crural fascia and interosseous membrane consist of thin conductive fibrous tissues. Though they appeared dark in MR magnitude images due to weak MR signals, corresponding pixels in the reconstructed conductivity images were bright for their high conductivity values.

Thresholds of perception and pain for current injections vary depending on body parts. Since the knee has much smaller thresholds, we had to reduce the injection current amplitude in knee experiments. The multi-echo pulse sequence enabled us to perform the knee experiments using 3 mA injection current without further increasing the total scan time for more data averaging. In the adopted multi-echo sequence, we combined multiple echoes to increase image SNRs. We could also increase the total current injection time using the multi-echo sequence. This was possible since T2 values of the knee region were long enough for the multi-echo pulse sequence. We found that uses of the first two echoes were enough since combining all three echoes did not reduce the noise level in B_z images. For the calf, we could not observe any significant improvement in conductivity images using the multi-echo pulse sequence. This can be attributed to smaller T2 values of the muscles in the calf region. These results indicate that we should customize a pulse sequence design for each body part considering both bioelectromagnetics and MR physics.

From the results reported in this study, we suggest always applying a chemical shift artifact correction in animal and human MREIT imaging experiments. Since conventional correction methods are for magnitude images, the correction method in MREIT must be properly customized for phase images [8,14,15]. For applications of fast sequences such as the fast spin echo (FSE) and steady state free precession (SSFP) in MREIT, we should use a more sophisticated water-fat separation method using small phase shifts of $\pm\alpha$ for $\alpha < \pi$ [16,17].

ACKNOWLEDGMENT

This work was supported by the National Research Foundation of Korea (NRF) grant funded by the Korea government (MEST) (No. 20100018275).

REFERENCES

[1] H. J. Kim, Y. T. Kim, A. S. Minhas, W. C. Jeong, E. J. Woo, J. K. Seo, O. J. Kwon, "In vivo high-resolution conductivity imaging of the human leg using MREIT: the first human experiment", IEEE Trans. Med. Imag., vol. 28, pp. 1681-1687, 2009.

[2] G. C. Scott, M. L. G. Joy, R. L. Armstrong, R. M. Henkelman, "Sensitivity of magnetic resonance current density imaging", J Magn. Reson., vol. 97, pp. 235-254, 1992.

[3] R. Sadleir, S. Grant, S. U. Zhang, B. I. Lee, H. C. Pyo, S. H. Oh, C. Park, E. J. Woo, S. Y. Lee, O. Kwon, J. K. Seo, "Noise analysis in magnetic resonance electrical impedance tomography at 3 and 11 T field strengths", Physiol. Meas., vol. 26, pp. 875-884, 2005.

[4] H. S. Nam, O. I. Kwon, "Optimization of multiply acquired magnetic flux density Bz using ICNE-multiecho train in MREIT", Phys. Med. Biol., vol. 55, pp. 2743-2759, 2010.

[5] Y. Q. Han, Z. J. Meng, W. C. Jeong, Y. T. Kim, A. S. Minhas, H. J. Kim, H. S. Nam, O. Kwon, E. J. Woo, "MREIT conductivity imaging of canine head using multi-echo pulse sequence", In: Proc. Int Conf on Elect Bioimpedance, Journal of Physics: Conference Series, vol. 224, pp. 012078, 2010.

[6] T. I. Oh, Y. Cho, Y. K. Hwang, S. H. Oh, E. J. Woo, S. Y. Lee, "Improved current source design to measure induced magnetic flux density distributions in MREIT", J Biomed. Eng. Res., vol. 27, pp. 30-37, 2006.

[7] C. Park, B. I. Lee, O. Kwon, E. J. Woo, "Measurement of induced magnetic flux density using injection current nonlinear encoding (ICNE) in MREIT", Physiol. Meas., vol. 28, pp.117-127, 2006.

[8] A. S. Minhas, Y. T. Kim, W. C. Jeong, H. J. Kim, S. Y. Lee, E. J. Woo, "Chemical shift artifact correction in MREIT", J Biomed. Eng. Res., vol. 30, pp. 461-468, 2009.

[9] K. Jeon, H. J. Kim, C. O. Lee, E. J. Woo, J. K. Seo, "CoReHA: conductivity reconstructor using harmonic algorithms for magnetic resonance electrical impedance tomography (MREIT)", J. Biomed. Eng. Res., vol. 30, pp. 279-287, 2009.

[10] J. K. Seo, S. W. Kim, S. Kim, J. J. Liu, E. J. Woo, K. Jeon, C. O. Lee, "Local harmonic Bz algorithm with domain decomposition in MREIT: computer simulation study", IEEE Trans. Med. Imag., vol. 27, pp. 1754-1761, 2008.

[11] W. T. Dixon, "Simple proton spectroscopic imaging", Radiology, vol. 153, pp. 189-194, 1984.

[12] G. H. Glover, E. Schneider, “Three-pointDixon technique for true water/fat decomposition with inhomogeneity correction”, Magn. Reson. Med., vol. 18, pp. 371-383, 1991.

[13] F. H. Netter, “Musculoskeletal system: anatomy, physiology, and metabolic disorders (Netter collection of medical illustrations)”, Saunders, 1988.

[14] M. J. Hamamura, O. Nalcioglu, L. T. Muftuler, “Correction of chemical shift artifact in magnetic resonance electrical impedance tomography”, In: Proc Intl Soc Magn Reson Med Conf, Honolulu, Hawai, USA, April 18-24, pp. 4658, 2009.

[15] S. B. Reeder, Z. Wen, H. Yu, A. R. Pineda, G. E. Gold, M. Markl, N. J. Pelc, “Multi-coil Dixon chemical species separation with an iterative least-squares estimation method”, Magn. Reson. Med., vol. 51, pp. 35-45, 2004.

[16] A. S. Minhas, E. J. Woo, S. Y. Lee SY, “Magnetic flux density measurement with balanced steady state free precession pulse sequence for MREIT: computer simulation study”, In: Proc. IEEE EMBC09, Minneapolis, MN, USA, Sept., pp 2276-2278, 2009.

[17] A. S. Minhas, E. J. Woo, R. Sadleir, “Simulation of MREIT using balanced steady state free precession (b-SSFP) pulse sequence”, In: Proc. Int Conf on Elect Bioimpedance, Journal of Physics: Conference Series, vol. 224, pp. 012019, 2010.